

Trends of Anthropogenic Dissolved Inorganic Carbon in the Northwest Atlantic Ocean Estimated Using a State Space Model

Claire Boteler¹ , Michael Dowd¹ , Eric C. J. Oliver² , Elias T. Krainski³ , and Douglas W. R. Wallace² 

¹Department of Mathematics and Statistics, Dalhousie University, Halifax, NS, Canada, ²Department of Oceanography, Dalhousie University, Halifax, NS, Canada, ³Department of Statistics, King Abdullah University of Science and Technology, Thuwal, Kingdom of Saudi Arabia

Key Points:

- A time series generalization of the extended multiple linear regression (eMLR) method is developed to produce monthly estimates with uncertainties of anthropogenic ocean carbon
- The rate of anthropogenic carbon increase in northwest Atlantic is roughly the same for all depth layers, at 0.57 $\mu\text{mol}/\text{kg}/\text{year}$
- Our method produces estimates of anthropogenic carbon increase that are comparable to those from eMLR, but with smaller uncertainties

Supporting Information:

Supporting Information may be found in the online version of this article.

Correspondence to:

C. Boteler,
claire.boteler@dal.ca

Citation:

Boteler, C., Dowd, M., Oliver, E. C. J., Krainski, E. T., & Wallace, D. W. R. (2023). Trends of anthropogenic dissolved inorganic carbon in the Northwest Atlantic Ocean estimated using a state space model. *Journal of Geophysical Research: Oceans*, 128, e2022JC019483. <https://doi.org/10.1029/2022JC019483>

Received 13 NOV 2022

Accepted 15 JUN 2023

Author Contributions:

Conceptualization: Claire Boteler, Michael Dowd, Eric C. J. Oliver, Elias T. Krainski, Douglas W. R. Wallace

Formal analysis: Claire Boteler

Funding acquisition: Douglas W. R. Wallace

Methodology: Claire Boteler, Michael Dowd, Elias T. Krainski

Supervision: Michael Dowd, Eric C. J. Oliver, Douglas W. R. Wallace

© 2023. The Authors.

This is an open access article under the terms of the [Creative Commons Attribution-NonCommercial-NoDerivs](https://creativecommons.org/licenses/by/4.0/) License, which permits use and distribution in any medium, provided the original work is properly cited, the use is non-commercial and no modifications or adaptations are made.

Abstract The northwest Atlantic Ocean is an important sink for carbon dioxide produced by anthropogenic activities. However the strong seasonal variability in the surface waters paired with the sparse and summer biased observations of ocean carbon makes it difficult to capture a full picture of its temporal variations throughout the water column. We aim to improve the estimation of temporal trends of dissolved inorganic carbon (DIC) due to anthropogenic sources using a new statistical approach: a time series generalization of the extended multiple linear regression (eMLR) method. Anthropogenic increase of northwest Atlantic DIC in the surface waters is hard to quantify due to the strong, natural seasonal variations of DIC. We address this by separating DIC into its seasonal, natural and anthropogenic components. Ocean carbon data is often collected in the summer, creating a summer bias, however using monthly averaged data made our results less susceptible to the strong summer bias in the available data. Variations in waters below 1000m have usually been analyzed on decadal time scales, but our monthly analysis showed the anthropogenic carbon component had a sudden change in 2000 from stationary to an increasing trend at the same rate as the waters above. All depths layers had similar rates of anthropogenic increase of $\sim 0.57 \mu\text{mol kg}^{-1} \text{ year}^{-1}$, and our uncertainty levels are smaller than with eMLR results. Integration throughout the water column (0–3,500 m) gives an anthropogenic carbon storage rate of $1.37 \pm 0.57 \text{ mol m}^{-2} \text{ year}^{-1}$, which is consistent with other published estimates.

Plain Language Summary We need to measure the ocean sink for the CO_2 emitted by industrialized societies, and it is particularly important for the northwest Atlantic Ocean. The rate of carbon increase is often overshadowed by natural and seasonal variability. We introduce new statistical approaches to better estimate the rate of anthropogenic carbon that has accumulated due to human activities. Ocean carbon data is often collected in the summer, creating a summer bias, however using monthly averaged data made our results less susceptible to the strong summer bias in the available data. From 1993 to 2015 in the northwest Atlantic Ocean, anthropogenic carbon increased at $\sim 0.57 \mu\text{mol kg}^{-1} \text{ year}^{-1}$ within all depth-layers. Integration of results throughout the water column (0–3,500 m) gives an anthropogenic carbon storage rate of $1.37 \pm 0.57 \text{ mol m}^{-2} \text{ year}^{-1}$.

1. Introduction

A key element for climate change projection and for carbon emission policy is how effective the ocean is, and will be, in mitigating the effects of anthropogenic CO_2 emissions. The northwest Atlantic is one of the largest oceanic carbon sinks on an areal basis, taking in and storing large amounts of anthropogenic CO_2 (Khaliwala et al., 2013). There are several chemical, physical and biological factors that influence how much CO_2 the ocean takes up throughout the year. In the winter, cold winds cool the surface waters, increasing the solubility of CO_2 (Emerson & Hedges, 2008), which enhances dissolved inorganic carbon (DIC) concentrations in the surface layers as a result of air-sea gas exchange. Temperature also influences the physical uptake processes of the area, as cooling reduces stratification and facilitates the transport of DIC rich waters from the surface to the deeper waters. The shoaling of the mixed layer in the summer traps DIC rich waters in the subsurface ocean where it is no longer in contact with the atmosphere. While respiration will release CO_2 into the surface waters, phytoplankton will use CO_2 for photosynthesis. Strong, seasonal biological production also promotes seasonal uptake of CO_2 from the atmosphere, which is transported deeper via the biological carbon and mixed-layer pumps (Lacour et al., 2019).

Visualization: Claire Boteler
Writing – original draft: Claire Boteler
Writing – review & editing: Claire Boteler, Michael Dowd, Eric C. J. Oliver, Elias T. Krainski, Douglas W. R. Wallace

The column inventory of anthropogenic DIC is the depth-integrated amount of ocean carbon present as a result of human activities, reported on a per area basis. In the northwest Atlantic this was estimated at 160 mol m^{-2} in 2010, several times greater than the global average (Khatiwala et al., 2013). The global ocean's uptake of atmospheric CO_2 estimated in the last 10 years, as diagnosed from observations, has been increasing at a faster rate than the uptake estimated from ocean models (see Figure 9 in Friedlingstein et al. (2020)). Such inconsistencies motivate our goal of improving the estimation of uptake and storage of anthropogenic carbon for the northwest Atlantic, as determined directly from DIC observations.

Observational data from two main sources are used to study the ocean carbon cycle. The SOCAT data set provides near-surface ocean pCO_2 measurements made on research cruises and ships of opportunity (Bakker et al., 2016). This data set has been used to estimate air-sea fluxes on the global scale with methods ranging from neural networks (Landschützer et al., 2014) to atmospheric inversion (Rödenbeck et al., 2013, 2015) and interpolation (Goddijn-Murphy et al., 2015). The GLODAP data set provides discrete water sample measurements for the ocean interior (Lauvset et al., 2021). This data set has been used to estimate the build up of anthropogenic CO_2 in the oceans (Khatiwala et al., 2013; Lauvset et al., 2016; Sabine, 2004) and diagnose ocean transport of carbon (Holfort et al., 1998; Macdonald et al., 2003). Analyses of temporal changes have tended to use regression approaches (Bostock et al., 2013; Friis et al., 2005; Gruber et al., 2019), but also use mechanistic approaches based on ocean biogeochemical models (Carroll et al., 2022; Friedlingstein et al., 2020; Gerber & Joos, 2010). Our study focuses on the use of interior ocean DIC observations from GLODAP.

An important and long-standing research question is how to separate DIC into its natural and anthropogenic components (Sabine & Tanhua, 2010; Wallace, 2001), where anthropogenic typically refers to the excess DIC present in the ocean as a result of human activities (i.e., due to atmospheric CO_2 increases since preindustrial times). Multiple linear regression (Wallace, 1995), and especially the extended Multiple Linear Regression method (eMLR) (Friis et al., 2005), are now widely used to estimate the increase of anthropogenic DIC. This is usually done between two time points that are a decade or more apart and on repeat hydrographic sections (Thacker, 2012). This approach has been extended recently to include eMLR in a depth-spatial moving window (Carter et al., 2017), eMLR for column inventories (Plancherel et al., 2013), and eMLR(C*) (Clement & Gruber, 2018). eMLR approaches are based on exploiting the changing relationship between observed DIC and other correlated ocean variables that are not directly impacted by anthropogenic CO_2 uptake, such as temperature, salinity and oxygen. The eMLR(C*) approach, for example, incorporates more ocean predictor variables and centers the analysis on a derived variable, called C*, that more closely relates to anthropogenic carbon than DIC. The eMLR based methods have proven to be useful for estimating trends over long time intervals (decades) in the sub-surface waters, but few studies have attempted an observation-centric analysis of DIC variations on shorter time scales. In addition, they have also not provided for reliable estimates in the surface ocean. This study aims to rectify those shortcomings and improve our understanding of ocean DIC.

The main challenges to quantifying the temporal variability of the carbon sink and the carbon inventory include: the seasonal variability that is particularly strong in the surface waters, observation sparsity, and a strong bias toward summer sampling (Fassbender et al., 2018; McKinley et al., 2017). There is potential for use of improved time series approaches to optimally extract information from existing DIC observational databases to improve our quantification of DIC dynamics over multiple time scales. Gruber (2002) has, for example, used time series methods that incorporate deseasonalization via harmonic analysis, fitting of linear trends, and analyzing correlations between variables. In this study, we build upon and generalize the eMLR method into a time series framework using dynamic linear regression. This allows us to analyze seasonally biased observations of DIC and isolate its sources of variability, while improving temporal resolution of the analysis and producing objective observation-driven error estimates. Our method provides estimation of anthropogenic changes in DIC, making it capable of assessing non-linear trends in anthropogenic CO_2 uptake, as well as its seasonal and inter-annual variability. Here, we use this approach to study DIC in the northwest Atlantic within three depth-layers ranging from the surface to the deep waters, and estimate on a monthly time scale the seasonal, natural variability and anthropogenic DIC. We also investigate the influence of seasonally biased observations on the analysis and results. This provides a North Atlantic perspective to complement the work performed with seasonally biased data in the Southern Ocean (Fassbender et al., 2018; Mackay et al., 2022).

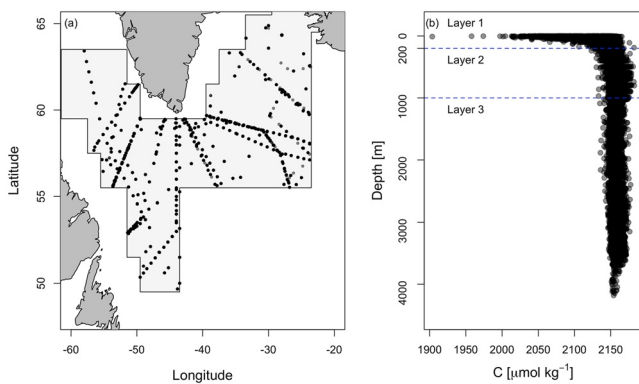


Figure 1. Spatial distributions of GLODAPv2.2019 data. (a) Geographical location of observations (semi-transparent gray dots). Repeated observations at the same location or at multiple depths or times are plotted on top of each other (appearing as solid black dots). The Atlantic Arctic Longhurst Province is indicated (gray polygon). (b) Observations of DIC versus depth are given. Horizontal dashed lines identify the 200 and 1,000 m depths that separate our data into three depth-layers.

2. Data

The principal data set used in this study is the GLODAPv2.2019 data product (Olsen et al., 2016, 2019), hereafter referred to as GLODAP. It is a global collection of quality controlled in situ measurements from scientific cruises conducted from 1972 to 2017. It contains 12 core biogeochemical variables, including our target variable of Dissolved Inorganic Carbon (DIC), which were measured from bottle samples and include their time and location coordinates (i.e., date, latitude, longitude and depth). Physical variables also reported include potential temperature and practical salinity; we make use of these two variables in our analysis because they have a strong mechanistic and statistical connection with DIC, are widely available, and are commonly used in eMLR analyses (Friis et al., 2005). The remaining biogeochemical variables have less frequent in situ measurements than temperature and salinity, and were chosen not to be included in this analysis. Hence, we considered only DIC and covariates of temperature and salinity in our analysis, although we note that in the future measurements of biogeochemical variables, such as oxygen from profiling floats, could be used with our approach to improve results.

Our region of interest is the northwest Atlantic, which we define as the region south of 65° N within the Atlantic Arctic (ARCT) Longhurst biogeochemical province (Longhurst, 2007) (Figure 1a). It includes areas of deep convection that are associated with intense anthropogenic carbon storage (Raimondi et al., 2021). These areas of deep convection have been shown to shift their location and intensity in space and time (Rühs et al., 2021). The relatively broad study area was chosen to ensure we captured all key regions of deep convection, as well as the more pragmatic concern of having a large enough data set for our analysis.

We separated the data into three depth-layers: layer 1: 0–200m, layer 2: 200–1,000 m, and layer 3: 1,000–4,500 m. These correspond to the euphotic zone (sunlit), the mesopelagic zone (twilight) and the bathypelagic zone (midnight), respectively (Berger & Shor, 2009). Biogeochemical ocean regions transition from surface to intermediate and deep waters at different depths due to the mixed layer depth which varies seasonally, interannually and spatially, and can be challenging to define quantitatively (Rühs et al., 2021). For this analysis the depths of layer boundaries were chosen to be constant through the year, and correspond to how the mean and standard deviation of DIC changed with depth (Figure 1b). The near surface, layer 1, has the largest spread of DIC due to direct gas exchange with the atmosphere and the seasonal biological activity that occurs in the euphotic zone (mean 2,124 $\mu\text{mol kg}^{-1}$ and standard deviation 31 $\mu\text{mol kg}^{-1}$). The separation between layer 1 and layer 2 at 200 m is similar to that used by others (Brewer et al., 1995; Turk et al., 2017; Ullman et al., 2009), as is the separation between layer 2 and layer 3 around 1,000 m (Bostock et al., 2013; Emery, 2001; Keppler et al., 2020). In layer 2 the mean DIC value becomes more constant and with a large reduction in spread (mean 2,158 $\mu\text{mol kg}^{-1}$ and standard deviation 8.6 $\mu\text{mol kg}^{-1}$). The deep layer 3 has an even smaller spread with a near-constant DIC (mean 2,159 $\mu\text{mol kg}^{-1}$ and standard deviation 5.6 $\mu\text{mol kg}^{-1}$).

The DIC observations from January 1993 to December 2015 have a distinct seasonal sampling bias, which is clearly seen in the distribution of observations by month (Figure 2a). Of the individual observations, 37% were recorded in the summer (July to October) while only 2% were recorded in the winter (Jan to Apr). The seasons are defined as the 4 months with the warmest and coldest temperatures in the ocean surface layer. Figure 2b shows DIC observations over time in the northwest Atlantic and highlights the difference between winter and summer, with summer having lower DIC values due to higher sea surface temperatures causing some outgassing but mainly due to phytoplankton photosynthesis using CO_2 (Montes-Hugo et al., 2010) in the surface waters. Fitting a linear temporal trend using least squares regression to the winter observations shows it is increasing at $0.77 \pm 0.07 \mu\text{mol kg}^{-1} \text{ year}^{-1}$, a faster rate than the $0.23 \pm 0.41 \mu\text{mol kg}^{-1} \text{ year}^{-1}$ for the summer observations. Figure 2b motivated the question of whether winter and summer really have different DIC trends, or if this is an artifact of sampling bias. This will be explored in Section 4.1. We pre-processed the data by separating it into the three depth-layers, after which each subset was turned into monthly averaged time series (which still have observation gaps). The monthly data was better balanced in terms of its seasonal distribution, that is, of the months

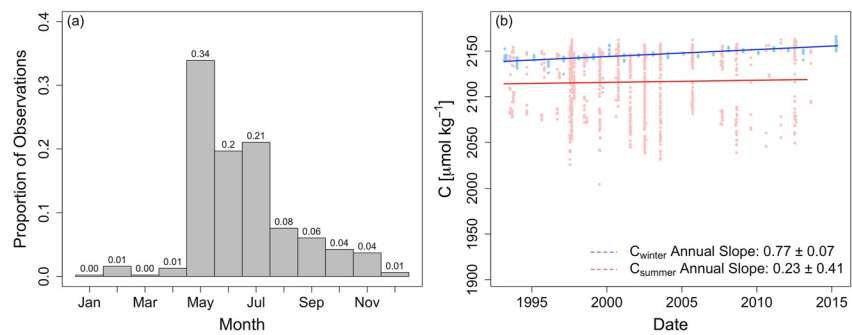


Figure 2. (a) Proportion by month of GLODAPv2.2019 DIC observations for depths 0–200m. Numbers at the top of each bar gives the proportion of observations occurring in that month. (b) Dissolved inorganic carbon (DIC) over time in the Northwest Atlantic domain for depths 0–200 m. Dots are colored by the season they were recorded: winter that is, January to April (blue dots), and summer that is, July to October (red dots). Note that spring and fall are not shown. To each of the different subsets, linear temporal trends were fitted using ordinary least squares, and their slopes are reported in units of $\mu\text{mol kg}^{-1} \text{ year}^{-1}$.

occurring in winter between 1993 and 2015, 8% had at least 1 observation and likewise 12% in summer had at least one observation. By averaging all observations in a month, this implicitly assumed that the observations in that month had homogeneous oceanographic properties, which is a viable assumption for our data contained within the Atlantic Arctic Longhurst Province.

GLODAP has many data gaps through time (Figure 2a). Our analysis has DIC as its target variable but, like the eMLR method, makes use of temperature and salinity as covariates to better estimate it. To improve the spatial and temporal coverage of temperature and salinity, we used the GLORYS12v1 reanalysis product to provide a complete time series for these physical oceanographic variables (GLORYS12V1 - Global Ocean Physical Reanalysis Product, 2018). GLORYS12v1 provides potential temperature and practical salinity values over a regular $1/12^\circ$ spatial grid, at 50 vertical depth-levels and on daily time intervals from 1993 to 2018. As with the GLODAP data, this daily reanalysis product was separated into our three depth-layers and converted into times series of monthly and spatially averaged values within our region of interest in the northwest Atlantic. Figure S2 in Supporting Information S1 shows that deseasonalized values for temperature and salinity from both GLODAP and GLORYS12v1 agree, with GLODAP having a slightly larger scatter, but are centered around the GLORYS12v1 values.

3. Methods

The eMLR method (Friis et al., 2005) has been widely used to estimate the anthropogenic increase of DIC between two time points, typically a decade or more apart. For a repeat-sampled ocean transect and assuming the relationship between the natural variability of DIC and oceanographic variables remains constant over time, any changes in the regression coefficients of the relationship can be interpreted as a non-natural change, that is, excess DIC due to anthropogenic sources (Thacker, 2012). When this is evaluated for the later time point, it yields an estimate of the anthropogenic increase of DIC over the time interval of study.

Here we develop and apply a time series generalization of the eMLR method. We build upon the eMLR methodology by using a time-invariant linear regression relationship of DIC against temperature and salinity to represent the natural variability of DIC, and we also include a time-varying term to represent the excess DIC. As with the eMLR method, we seek to quantify the change in DIC over time, but ours is a time series method that better resolves the changes through time. While the eMLR looks at differences over a fixed time interval, our time series approach constrains variability over a range of time scales, and allows us to look at inter-annual to decadal variability of anthropogenic DIC. It can also account for common observational issues such as varying sampling intervals and data gaps. Importantly, it can produce statistically objective error bars that change through time and reflect the data properties and distribution. Our approach, as detailed below, is based on a decomposition of the DIC observations into three components: a seasonal cycle, natural variability, and excess carbon due to anthropogenic sources. It produces monthly time series of these carbon components (with confidence intervals).

3.1. Decomposition of DIC

We designate DIC observations as C_t . The first step was to deseasonalize them, such that

$$C'_t = C_t - C_t^s \quad (1)$$

where C'_t are the deseasonalized DIC anomalies and C_t^s represents the mean seasonal cycle over the period of interest. This seasonal cycle, C_t^s was estimated empirically by taking the mean of each month (Jan, Feb, etc.). The equivalent deseasonalization procedure was also performed for our other variables of temperature T_t and salinity S_t . The DIC anomalies were then further decomposed as follows:

$$C'_t = C_t^e + C_t^n + v_t \quad (2)$$

where C_t^e represents the excess carbon (e.g., assumed due to anthropogenic sources) and C_t^n represents the natural variability (e.g., from variations in oceanic water properties). The v_t is called the observation error, and contains the remaining variability not described by the excess and natural variability components, that is, within-month variations, and measurement error. Separating the natural and anthropogenic changes of DIC in Equation 2 is the same concept proposed in Clement and Gruber (2018), but the methods used to estimate the natural and anthropogenic components target different parts of the carbon system, that is, circulation and mixing, biological pump, solubility pump, and air-sea flux, and will be discussed further in Section 5.

In order to separate and estimate the excess carbon and natural variability components, we build upon foundational assumptions of the eMLR method and re-cast Equation 2 as the regression equation

$$C'_t = \beta_{0,t} + \beta_1 T'_t + \beta_2 S'_t + v_t. \quad (3)$$

The excess DIC, C_t^e , is now represented by the time varying intercept term $\beta_{0,t}$. The natural variability, C_t^n , is equated with the terms $\beta_1 T'_t + \beta_2 S'_t$, representing a linear relationship between anomalies of DIC and anomalies of temperature, T'_t , and salinity, S'_t . Note, the linear regression could be expanded to include biogeochemical ocean variables such as oxygen, etc. We assumed observation error $v_t \sim N(0, \sigma_v^2)$. For this time-dependent regression, we estimated the four parameters: $\beta_{0,t}$, β_1 , β_2 , and σ_v using the monthly averaged and deseasonalized GLODAP DIC data.

To illustrate how our method relates to the equations used in the eMLR method, consider the eMLR prediction equation for anthropogenic carbon (C^{eMLR}) that has been expanded to show its two regressions:

$$\begin{aligned} C^{eMLR} &= (a_{t_2} - a_{t_1}) + (b_{t_2} - b_{t_1})T_{t_2} + (c_{t_2} - c_{t_1})S_{t_2} \\ &= (a_{t_2} + b_{t_2}T_{t_2} + c_{t_2}S_{t_2}) - (a_{t_1} + b_{t_1}T_{t_2} + c_{t_1}S_{t_2}). \end{aligned}$$

The regression parameters a_{t_1} , b_{t_1} and c_{t_1} would be estimated from DIC, temperature and salinity data at time t_1 , and similarly for parameters a_{t_2} , b_{t_2} and c_{t_2} estimated at time t_2 . Both regressions are predicted at T_{t_2} and S_{t_2} , temperature and salinity at time t_2 . When the eMLR is expanded to show its two regressions, the second bracket ($a_{t_1} + b_{t_1}T_{t_2} + c_{t_1}S_{t_2}$) is equivalent to our natural component but evaluated at each time t in our monthly time series. The anthropogenic carbon (C^{eMLR}) is equivalent to our time varying intercept term ($\beta_{0,t}$).

3.2. Dynamic Linear Regression

To estimate excess carbon, C_t^e via $\beta_{0,t}$, we used a state space modeling framework that corresponds to dynamic linear regression (Laine, 2020; Zivot & Wang, 2003). This uses two equations: an observation equation (as described by Equation 3 above) and a prediction equation (as described by Equation 4 below). The prediction equation predicts the time evolution of excess carbon, as embodied in the regression intercept $\beta_{0,t}$. It takes the form

$$\beta_{0,t} = \beta_{0,t-1} + \phi(\beta_{0,t-1} - \beta_{0,t-2}) + w_t. \quad (4)$$

This is a correlated random walk process. It predicts the excess carbon at time t ($\beta_{0,t}$) based on its previous two values at times $t - 1$ and $t - 2$. Specifically, the update is based on $\beta_{0,t-1}$ plus a proportion of the change occurring between the previous two time steps ($\beta_{0,t-1} - \beta_{0,t-2}$). Note that the unit time increments used here refer to the time interval of the analysis, in this instance monthly. The parameter ϕ is a measure of the strength of the excess

Table 1
Dynamic Linear Regression Parameters Estimated for Each Depth-Layer

	$\hat{\beta}_{0,t=1}$	$\hat{\beta}_1$	$\hat{\beta}_2$	$\hat{\sigma}_{\epsilon,t=1}$	$\hat{\sigma}_v$	$\hat{\sigma}_w$	$\hat{\phi}$
Layer 1: 0–200 m	−5.40	−6.97	47.72	2.0	10.1	0.10	0.64
Layer 2: 200–1,000 m	−4.17	0	0	1.7	2.2	0.95	0
Layer 3: 1,000–4,500 m	−2.73	7.40	0	1.5	6.5	0.10	0.46

carbon time tendency; we term this the *proportion of trend persistence*. Note that we used a random walk instead of an auto-regressive process for the prediction (Equation 4) because such a stationary autoregressive processes have a mean reversion property (i.e., when predicting forward in time, they are drawn back to the mean), which is inconsistent with the increasing anthropogenic DIC over time that we wish to quantify. The purpose of the correlated random walk is to introduce temporal memory in excess carbon, with the DIC observations guiding its time evolution through the state space model Equations 3 and 4. The prediction error for the new intercept is given by $w_t \sim N(0, \sigma_w^2)$, and its variance σ_w^2 will be estimated as part of the implementation (see Section 3.3).

The Kalman filter/smoothing algorithm (see, e.g., Anderson & Moore, 1979) was used to solve this dynamic linear regression Equations 3 and 4. This fixed-interval smoother provides for estimation of the system state, which in this instance is excess carbon, $\beta_{0,t}$. Specifically, it provides for the monthly estimates of the mean values of excess carbon and its time-varying variance. The variance can be used to produce errors bars, that is, confidence intervals for excess carbon. The algorithm uses sequential, or recursive, estimation. This relies on the Kalman filter, which operates as a forward in time recursion such that at each time step t , an estimate of the new excess carbon value is available via a one-step ahead prediction using Equation 4. This prediction is then updated to be closer to the DIC observation using a smoother step that further refines these estimates through a backwards in time recursion. The ratio of the variances for the observation error (σ_v) to the prediction error (σ_w) is a key quantity that dictates how closely the results follow the observations. To facilitate their specification, the Kalman filter also allows for parameter estimation through likelihood-based approaches. For this study, we estimated the parameters ϕ and σ_w^2 using maximum likelihood, while σ_v was estimated from analysis of DIC observations. For details of the Kalman filter/smoothing and parameter estimation, the reader is referred to the Supplementary Information.

3.3. Implementation

To implement our proposed methodology, the following steps were taken to perform the analysis on each depth-layer. Following the pre-processing of the DIC, T and S data into monthly average time series, we: (i) determine the seasonal cycle, and deseasonalize DIC, T and S; (ii) find the regression coefficients relating DIC to T and S, that is, $\beta_{0,t=1}$, β_1 and β_2 ; (iii) specify initial conditions for mean and variance of excess carbon; (iv) specify or estimate the state space model parameters: σ_v , σ_w and ϕ ; (v) carry out state estimation of excess carbon component with Kalman Smoother; (vi) reconstruct the total carbon time series by combining its components (excess, natural, seasonal). These steps are outlined in detail below.

(i) Seasonal Component and Deseasonalize DIC, T, and S

After pre-processing the data into a monthly average time series, the seasonal cycle of DIC, \hat{C}_t^s , was estimated from the GLODAP monthly observations as the long-term mean for each month (e.g., the mean of all Januaries across all years of data). The seasonal cycle of DIC was removed to produce observations of deseasonalized DIC anomalies, C'_t . The temperature and salinity observations were also deseasonalized to yield T'_t and S'_t .

(ii) Estimate Regression Coefficients That Relate C'_t to T'_t and S'_t : $\beta_{0,t=1}$, β_1 , and β_2

The regression coefficients $\hat{\beta}_{0,t=1}$, $\hat{\beta}_1$, and $\hat{\beta}_2$ from Equation 3 were estimated with ordinary least squares regression using deseasonalized GLODAP data from the first five years (1993–1997). When estimating the regression parameters for the covariates, it was important to check the overall regression significance (F -test), and the significance for each parameter (t -test). If the regression was not significant, then the natural component become a constant value set to 0 and we set $\hat{\beta}_1 = \hat{\beta}_2 = 0$, as is seen in Table 1. In the case that one parameter was not significant then that parameter was set to 0 (e.g., $\hat{\beta}_2 = 0$), effectively simplifying the regression to have only one covariate.

The 5 year time span was chosen to provide enough data to estimate a statistically significant regression, but small enough that we could assume the anthropogenic changes of carbon within the time span were negligible.

The relationship between carbon and its covariates change over time, such that if regressions on the first 5 years and the last 5 years were performed, their estimated parameters would be different, which is the foundation of the eMLR method (Friis et al., 2005). We took the eMLR assumption that *the natural relationship of carbon with covariates does not change over time* literally by using data at only the beginning of the analysis period in order to establish the baseline natural oceanographic relationship between DIC and temperature and salinity, that would not take into account anthropogenic changes over time.

(iii) Initial Conditions for Mean and Variance of Excess Carbon

To run the sequential Kalman smoother algorithm, we require an initial condition for the mean and variance of the state. The initial condition for its mean, $\hat{\beta}_{0,t=1}$, was estimated in the previous step with the other regression coefficients, using ordinary least squares regression with the deseasonalized GLODAP data from the first two years (1993–1997). For the initial condition of its variance $\hat{\sigma}_{e,t=1}^2$ a reasonable value is selected by iterating through Sections 3.3.3–3.3.5 a couple of times for an initial variance that did not artificially inflate or deflate the confidence intervals of excess carbon.

(iv) Estimate State Space Model Parameters: σ_v , σ_w and ϕ

The observation error standard deviation, σ_v , was derived from deviations of the original DIC observations, C , about the estimated seasonal cycle. Specifically, standard errors for each of the 12 months were calculated from the original GLODAP observations for the duration of the analysis period. The median of these values was used as $\hat{\sigma}_v$ and are reported in Table 1. (Note that this standard error is for monthly mean values and hence corresponds to what is here termed the observation standard deviation of DIC anomalies C'_t).

Parameter estimates for the prediction standard deviation, σ_w , and the proportion of trend persistence, ϕ , were determined using the method of maximum likelihood. The likelihood is determined by using the one-step ahead predictions of the Kalman filter, and its detailed computation is outlined in the Supporting Information S1. The maximum likelihood parameter values for ϕ and σ_w are given in Table 1.

(v) State Estimation of Excess Carbon With Kalman Smoother

We execute the dynamic linear regression Equations 3 and 4 with the Kalman smoother algorithm, producing a monthly estimate of the excess carbon component $\hat{\beta}_{0,t}$ and its variance $\hat{\sigma}_{e,t}^2$, which was used to construct 95% confidence intervals. Details of the Kalman smoother are provided in the Supporting Information S1.

(vi) Reconstructing Total Carbon

The total carbon time series was reconstructed by combining estimates for its seasonal, natural and excess components. The natural variability component within Equation 3 is estimated using the regression parameters $\hat{\beta}_1$ and $\hat{\beta}_2$ along with deseasonalized temperature and salinity from a prediction data set ($\hat{C}_t^n = \hat{\beta}_1 T'_{p,t} + \hat{\beta}_2 S'_{p,t}$). The GLORYS12v1 reanalysis product was used as the prediction data set. The errors of the natural component were calculated using the 95% prediction intervals from the linear regression, which is equivalent to the amount of variability that remains to be described by the excess carbon component.

As a final remark on error bars, by adding together the carbon components (seasonal, natural variability and excess carbon) we get a complete monthly time series estimate of total carbon ($\hat{C}_t = \hat{C}_t^s + \hat{C}_t^n + \hat{C}_t^e$). As the components are additive, so are the variances for natural variability and excess carbon, which produces a confidence interval for carbon anomalies. This uncertainty was also used for total carbon because we considered the deseasonalization done in Equation 1 as a linear transformation prior to our main analysis. For the seasonal component, confidence intervals ($1.96 \times$ the standard error of the seasonal cycle of DIC) show the within month variability that was considered for the estimation of the observation standard deviation ($\hat{\sigma}_v$). Table 1 gives estimates for all the parameters needed to initialize and execute the dynamic linear regression: the estimated initial regression coefficients ($\hat{\beta}_{0,t=1}$, $\hat{\beta}_1$, and $\hat{\beta}_2$), initial standard error ($\hat{\sigma}_{e,t=1}$), observation standard deviation ($\hat{\sigma}_v$), prediction standard deviation ($\hat{\sigma}_w$) and the proportion of trend persistence ($\hat{\phi}$).

4. Results

4.1. Carbon Components: Seasonal, Natural, and Excess

The seasonal evolution of DIC (\hat{C}_t^s) for our three depth-layers is shown in Figure 3. The surface water in layer 1 shows a prominent annual cycle peaking at $2,142 \mu\text{mol kg}^{-1}$ in the spring followed by the lowering of DIC

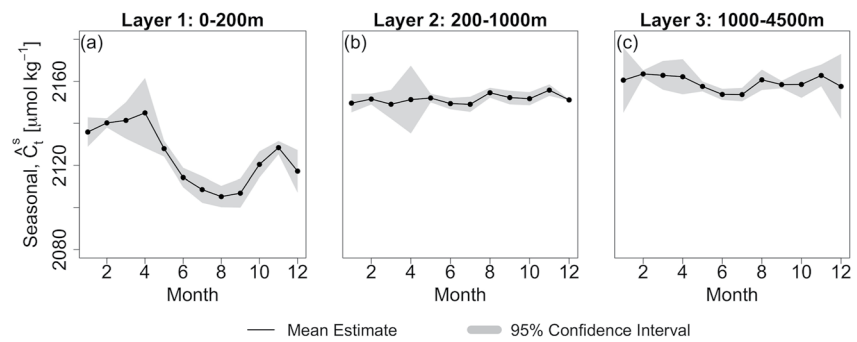


Figure 3. Seasonal cycle of DIC, \hat{C}_t^s , for each depth-layer: (a) layer 1: 0–200m, (b) layer 2: 200–1,000 m, and (c) layer 3: 1,000–4,500 m. Each plot shows the estimated mean (black line) and 95% confidence intervals (gray area).

corresponding to the spring bloom of phytoplankton. In the fall, DIC begins to rise again, aligning with the deepening of the mixed layer, incorporating waters with higher DIC values due to subsurface respiration. Layer 1 seasonal DIC showed a secondary peak in the fall at $2,133 \mu\text{mol kg}^{-1}$, however note there is large uncertainty associated with the dip in December. The deeper waters maintain a roughly constant value throughout the year. The annual average of the seasonal cycle in layer 2 is larger than in layer 1 (by $32 \mu\text{mol kg}^{-1}$) and for layer 3 it is slightly larger again (by $12 \mu\text{mol kg}^{-1}$). Layer 3 shows a subtle seasonal cycle that could possibly be related to changes through the year within the dominant water mass that flows into the region via boundary currents, similar to the seasonal signal discovered for oxygen concentrations in the deep Labrador Sea boundary current (Koelling et al., 2022). However, based on the width of the confidence interval, the seasonal cycle in layer 3 may not be statistically significant.

The natural variability component of carbon (\hat{C}_t^n) shows variations of DIC that are related to oceanic temperature and salinity variations (Figure 4), and captures the inter- and intra-annual variations of carbon. For the natural component in layer 3, the variations are very small with an amplitude of $1 \mu\text{mol kg}^{-1}$ and a significant trend of $0.07 \pm 0.04 \mu\text{mol kg}^{-1} \text{ year}^{-1}$ as estimated via generalized least squares regression. Layer 1 has no significant increasing trend, meanwhile its fluctuations have a larger amplitude of $7.9 \mu\text{mol kg}^{-1}$. Upon further inspection of the layer 1 natural component using spectral analysis, its statistical character changed at ~ 2006 from high frequency (i.e., periods shorter than a year) to low frequency (i.e., periods longer than a year) (Figure 4a). The natural component in layer 2 is shown as a constant line because a statistically significant regression relationship could not be estimated for DIC anomalies against temperature and salinity covariates (Table 1 shows $\hat{\beta}_1 = \hat{\beta}_2 = 0$). A non-significant regression relationship occurred due to the small amount of data used for fitting, and also the natural variability being small. The natural regression relationship for layer 1 used both temperature and salinity, while that for layer 3 used only temperature. The 95% prediction intervals show the amount of variability that remains to be described by the excess carbon component.

The excess components of carbon (\hat{C}_t^e) represent the increase of anthropogenic DIC over time, with the largest annual increase occurring in the surface waters. The anthropogenic increases are presented as a linear trend

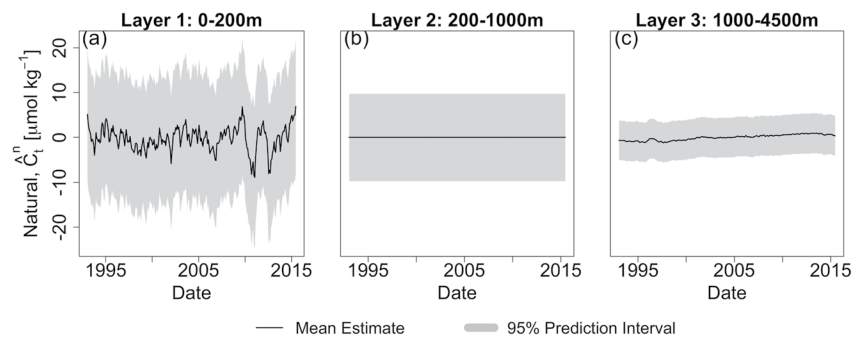


Figure 4. The natural variability component of carbon, \hat{C}_t^n , for each depth-layer: (a) layer 1: 0–200 m, (b) layer 2: 200–1,000 m, and (c) layer 3: 1,000–4,500 m. Each plot shows the estimated mean (black line) and 95% prediction intervals (gray area).

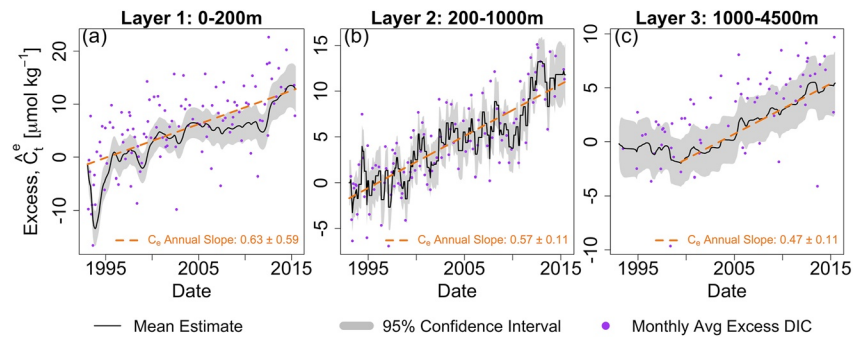


Figure 5. The excess carbon component, \hat{C}_t^c , for each depth-layer: (a) layer 1: 0–200 m, (b) layer 2: 200–1,000 m, and (c) layer 3: 1,000–4,500 m. Each plot shows the estimated mean (black line) and 95% confidence intervals (gray area). Monthly averaged excess DIC (i.e., C_t^c) are DIC anomalies after removing the seasonal and natural components) are also shown (purple dots). Annual trends are shown for excess DIC (orange dashed line), and their slopes are reported in the legend in units of $\mu\text{mol kg}^{-1} \text{ year}^{-1}$.

for convenience, and fit using generalized least squares. Considering their confidence intervals overlap, all three layers have approximately the same rate of increase of $\sim 0.57 \mu\text{mol kg}^{-1} \text{ year}^{-1}$ (Figure 5). Specifically, the trend in layer 1 is $0.63 \pm 0.59 \mu\text{mol kg}^{-1} \text{ year}^{-1}$, layer 2 is $0.57 \pm 0.11 \mu\text{mol kg}^{-1} \text{ year}^{-1}$, and layer 3 is $0.47 \pm 0.11 \mu\text{mol kg}^{-1} \text{ year}^{-1}$. However, the layer 3 trend was only estimated using 2000–2015 data. Prior to 2000, the excess carbon component had a slight declining trend, though it was not statistically significant. The apparent difference in trend before and after 2000 is notable, and is suggestive of low frequency variability in the ventilation of the deep ocean.

The time series characteristics of excess carbon in layer 2 (Figure 5b) are influenced by the observations and the input parameters used for the dynamic linear regression (i.e., σ_v , σ_w , and ϕ). The maximum likelihood procedure estimated the trend persistence to be zero ($\phi = 0$), which suggests that excess carbon in this layer follows a random walk, instead of a correlated random walk (when $\phi \neq 0$). This leads to a more blocky and erratic (rather than smoothly varying) appearance. Excess carbon in layer 1 and 3 have smoother inter-annual variations due to following a correlated random walk through the observations ($\phi = 0.64$ and 0.46 , respectively). In layer 3, the observations are less frequent, commonly with 3–5 month gaps, resulting in sections with a subtle staircase appearance with the Kalman smoother predicting the same value over the observation gaps (e.g., years 2000–2005).

As a naive test for sampling bias, a linear trend was estimated for the reconstructed total carbon over time. Similar trends were obtained regardless of the subset of months used of our carbon estimate, thus supporting that we have accounted for the data's sampling bias. In contrast, trend analysis of individual GLODAP observations (not monthly averages) produced very different results for different subsets (i.e., only winter or only summer data). The largest influence in accounting for seasonal sampling bias was the pre-processing step of monthly averaging the data.

4.2. Comparison to eMLR

We now compare the results from our statistical approach with those obtained using the eMLR approach. We ran an eMLR analysis with potential temperature and practical salinity to estimate the increase of anthropogenic carbon in the study region using GLODAP data from the first two years (1993–1994) and the last two years (2015–2016); spatial plots of the data used are shown in Figure S3 in Supporting Information S1. The eMLR anthropogenic increase over 24 years was estimated for layer 1, layer 2, and layer 3 to be 0.52, 0.49, and $0.47 \mu\text{mol kg}^{-1} \text{ year}^{-1}$, respectively. These eMLR results agreed generally with other eMLR results from Friis et al. (2005), who reported results between 0.4 and $1.6 \mu\text{mol kg}^{-1} \text{ year}^{-1}$ for transects in the same overall region of the North Atlantic.

We then compared these eMLR results with our excess carbon results from dynamic linear regression; the rates of increase for layer 1, layer 2 and layer 3 were 0.63 ± 0.59 , 0.57 ± 0.11 , and $0.47 \pm 0.11 \mu\text{mol kg}^{-1} \text{ year}^{-1}$, respectively (from Figure 5). For layer 3, both the eMLR and dynamic linear regression report the same rate of

increase of $0.47 \mu\text{mol kg}^{-1} \text{ year}^{-1}$. For layers 1 and 2, our dynamic linear regression results gave faster increases than the eMLR results, but the eMLR results are within our confidence intervals. Our method produces roughly equivalent rates of overall anthropogenic increase as eMLR, but are resolved on a monthly time scale providing information on climate-related changes in DIC over time.

4.3. Column Inventories of Carbon

We converted our estimate of excess carbon concentration (\hat{C}_t^e in units of $\mu\text{mol kg}^{-1}$) into column inventories of anthropogenic carbon (I_t), that is, depth-integrated carbon per unit area (in units of mol m^{-2}). The purpose was to facilitate comparison with other values in the literature, which are often reported as column inventories. The conversion $I_t = \rho H \hat{C}_t^e$ used the average density of seawater $\rho = f(T, S, P)$ and the layer thickness (H). For layer 3, which has observations from 1,000 to 4,500 m, its layer thickness was calculated with an ocean bottom depth of 3,500 m, which was the median bottom depth associated with GLODAP observations. The conversion to I_t produced a time series of mean column inventory in our study region that looks the same as Figure 5. The difference between the maximum and minimum values gave estimates for the excess carbon storage per square meter for each layer: 5.55 mol m^{-2} for layer 1 (0–200 m), 13.86 mol m^{-2} for layer 2 (200–1,000 m), and 20.63 mol m^{-2} for layer 3 (1,000–3,500 m). The time series for the three depth-layers were then added together and the difference between its maximum and minimum values gave an overall excess carbon storage of 35.41 mol m^{-2} through the whole water column over the period 1993 to 2015, corresponding to an average storage rate of $1.54 \text{ mol m}^{-2} \text{ year}^{-1}$. A conservative storage rate of $1.37 \pm 0.57 \text{ mol m}^{-2} \text{ year}^{-1}$ was estimated as the slope ($\pm 95\%$ confidence interval) of a linear generalized least squares regression through the time series for the whole water column (i.e., the combined layers). Note, this water column estimate is strongly influenced by the excess carbon time series in layer 3 due to its very large layer thickness.

Our estimated storage rate of excess carbon of $1.37 \pm 0.57 \text{ mol m}^{-2} \text{ year}^{-1}$, when considering the width of its confidence interval, is consistent with the average storage rate of $1 \text{ mol m}^{-2} \text{ year}^{-1}$ approximated from Figure 3A in Gruber et al. (2019) for our study region. Our confidence interval also overlaps with the reported estimate and uncertainty of $0.97 \pm 0.34 \text{ mol m}^{-2} \text{ year}^{-1}$ for DIC storage rate in the subpolar northwest Atlantic above 2000m (Tanhua & Keeling, 2012), as well as those for the Irminger Sea, where Fröb et al. (2018) reports the increase of anthropogenic carbon at $1.84 \pm 0.16 \text{ mol m}^{-2} \text{ year}^{-1}$. The time spans of study were similar: 1994–2007 (Gruber et al., 2019), 1980–2010 (Tanhua & Keeling, 2012), 1991–2015 (Fröb et al., 2018) and 1993–2015 for our study. Differences might be accounted by our data pre-processing step of spatially and monthly averaging data across a large region spanning both the Labrador Sea and Irminger Sea, while Gruber et al. (2019) and Fröb et al. (2018) analyzed column inventories on a smaller spatial grid. While spatial sampling bias across the large study region may affect our estimates, it nonetheless serves to demonstrate the analysis method while highlighting and mitigating data availability complications, such as seasonal sampling bias.

5. Discussion and Conclusions

Our time series generalization of the eMLR method is based on a dynamic linear regression (a state space model) that incorporates time dependence, accounts for irregular temporal sampling of data, and provides for an assessment of estimation errors based on observation properties. We then analyzed the temporal trends and variability of DIC on a monthly basis and estimated the anthropogenic increase of DIC in a manner that accounts for the strong seasonal sampling bias of the input data. We improved the temporal resolution of anthropogenic carbon estimates from being a simple difference between two widely separated time periods with eMLR (Carter et al., 2017; Friis et al., 2005) to providing DIC estimates on a monthly time scale. This allows the opportunity to look at inter-annual variability and elucidate connections between excess carbon uptake and climate forcing or circulation changes. We were also able to present improved estimates of the anthropogenic component of DIC in the surface layer by accounting for the strong seasonal variations, which usually interfere.

For the northwest Atlantic we produced monthly time series estimates of DIC, with uncertainties, including estimates for the seasonal cycle, natural variability and excess anthropogenic carbon components. The annual increase of excess carbon due to anthropogenic sources since 2000 was estimated at $\sim 0.57 \mu\text{mol kg}^{-1} \text{ year}^{-1}$ for all depth-layers. Our estimated storage rate, through the full water column (0–3,500 m), of anthropogenic carbon was $1.37 \pm 0.57 \text{ mol m}^{-2} \text{ year}^{-1}$, which seems consistent with the $1 \text{ mol m}^{-2} \text{ year}^{-1}$ shown in Figure 3A of Gruber et al. (2019) for our study region.

While we summarize our results with linear trends it brings into question whether a linear trend could be used directly in Equation 3 to model anthropogenic carbon instead of a correlated random walk (i.e., the time-varying intercept term $\beta_{0,t}$). Though a linear trend in the model would provide for similar estimates of the rate of anthropogenic carbon increase, the correlated random walk provides a framework that allows the state variable to follow the data through its inter-annual variations while not constraining the data to follow a straight line. As seen in Figure 5c, the trend is not linear for the whole time frame of analysis, with an increase in excess carbon after 2000 but not before. The flexibility of the correlated random walk framework also can show excess carbon variations at sub-seasonal time scales.

Our excess carbon component describes most of the anthropogenic change of DIC in the northwest Atlantic, but potentially not all of it. Global ocean temperatures are warming and salinity in the subpolar North Atlantic is freshening (Sathyanarayanan et al., 2021). These anthropogenic changes in temperature and salinity can then influence what is here defined as the natural variability component of carbon. Our natural variability component for layer 3 (Figure 4c) shows an increasing trend starting at the year 2000 that may reflect this anthropogenic influence, and could even be associated with the ‘warming hole’ of ocean temperature and changes in deep convection in the North Atlantic (Drijfhout et al., 2012). Hence, a benefit of our method is that it allows for the distinction between the anthropogenic change in ocean properties (i.e., temperature and salinity) and anthropogenic changes in DIC due to increasing CO₂ in the atmosphere. In contrast, Gruber et al. (2019) subtracted the non-steady state net flux of natural CO₂ associated with anthropogenic climate change such as ocean warming. Meanwhile, Fröb et al. (2018) estimated the natural DIC component in the Irminger Sea to have had a declining trend until 2015. This distinction of different sources of anthropogenic change may be important in the future because they might even drive opposing changes. For example, in the near-surface, the anthropogenic increase of atmospheric pCO₂ (partial pressure of CO₂) will increase ocean carbon, while warming ocean temperatures due to anthropogenic climate change lowers the solubility of CO₂ and may drive outgassing (Ciais et al., 2013).

By estimating a monthly time series of excess carbon, we are moving toward understanding variability of anthropogenic DIC on a finer time resolution. In our layer 1 excess carbon estimate, clusters of observations in 1993 and 2011 cause a dip below the decadal trend, and these clusters coincided with North Atlantic Oscillation (NAO) Index values above 2 (North Atlantic Oscillation, 2005). Connections between inter-annual variability of near-surface DIC and the NAO have been discussed in earlier studies (Gruber, 2002; Levine et al., 2011; Thomas et al., 2008; Ullman et al., 2009). Though variations of DIC at higher frequencies than annual are possible, they are rarely discussed due to data sparsity, which generally does not allow us to resolve these intra-annual variations with simpler time series methods.

The natural variability regression with temperature and salinity was investigated for its sensitivity to seasonally biased data. The regression was fit to four subsets of data, winter, spring, summer and fall. The parameters estimated (i.e., β_1 and β_2) were different for each subset. When all data was used the parameters estimated were equivalent to the average of the parameters from the seasonal subsets.

We reported our excess carbon estimates with 95% confidence intervals, however careful consideration is needed when comparing uncertainty measures with other studies and approaches. Confidence intervals are a common measure of uncertainty but in ocean carbon research other metrics are often used including: standard error and root mean squared error (RMSE) (Bittig et al., 2018; Clement & Gruber, 2018; Gruber et al., 2019; Landschützer et al., 2013; Plancherel et al., 2013), Gaussian propagation (Friis et al., 2005) or sum of error contributions and network weights for a Bayesian neural network (Bittig et al., 2018). Many who use these methods report errors as the deviations from their estimate, essentially a standard error (note 95% confidence intervals are: mean $\pm 1.96 \times$ standard error). For an eMLR analysis in a similar region to this study, Friis et al. (2005) reported anthropogenic carbon with errors of $\pm 7 \mu\text{mol kg}^{-1}$ in waters above 300 m and $\pm 3 \mu\text{mol kg}^{-1}$ in water below 300m. Our confidence intervals vary over time based on the availability of the observations but we can use the mean of our estimated standard error from the Kalman smoother. Our comparable excess carbon errors are: $\pm 1.6 \mu\text{mol kg}^{-1}$ in layer 1, $\pm 1.3 \mu\text{mol kg}^{-1}$ in layer 2, and $\pm 1.2 \mu\text{mol kg}^{-1}$ in layer 3. This implies that our uncertainty levels are smaller than with eMLR. Note also that our error estimates are anchored in maximum likelihood estimates of the key parameters in our state space model. Future work could focus on improvement of the uncertainty quantification by incorporating our multi-step analysis procedure into a comprehensive hierarchical statistical modeling framework (Cressie & Wikle, 2011).

In our approach, we separate DIC into its seasonal, natural variability and excess carbon components in Equations 1 and 2, with an emphasis on improving estimation of the increase in anthropogenic carbon, particularly its temporal aspects. Our goals are thus very similar to the eMLR(C*) method of Clement and Gruber (2018),

but there are important similarities and differences. (i) Our approach is designed to provide for detailed estimates of the evolution of anthropogenic carbon through time (i.e., monthly time series), whereas eMLR(C*), like the original eMLR, focuses on contrasting anthropogenic carbon content between widely separated time points (typically decades or longer). (ii) We do not make use of the C* variable to correct carbon concentrations for effects of biological activity, but rather emulate the original eMLR approach by using linear regression to separate natural and anthropogenic carbon. (iii) Both approaches recognize and account for the fact there can be variability and trends in both anthropogenic and natural carbon, unlike the original eMLR method. (iv) The final step in eMLR(C*) after training the regression models makes use of fields of climatological ocean variables as predictors thus allowing for highly resolved spatial estimates of anthropogenic carbon. There is undoubtedly considerable scope for the fusion of our dynamic linear regression method with many aspects of the eMLR(C*) approach to further improve anthropogenic carbon estimation.

Other candidate approaches for estimating DIC trends and variability include machine learning and biogeochemical modelling. Machine learning methods have risen in popularity and have been used to estimate the ocean carbon budget and air-sea CO₂ fluxes (Bittig et al., 2018; Broullón et al., 2020; Keppler et al., 2020; Landschützer et al., 2013). Machine learning methods, such as neural networks, focus on linking response variables to predictors by optimizing predictive skill and allowing for complex, non-linear relationships between variables. However, interpretation and diagnosis of cause and effect is often difficult. Due to this, machine learning is commonly used to gap-fill sparse observational ocean data (i.e., mapping). Both regression and neural network outputs can be used to investigate anthropogenic carbon trends, inter-annual variations, and seasonal variations. However, our component-based time series regression provides for clear interpretability of model results, and for statistical uncertainty estimates. Biogeochemical models, in contrast, provide detailed information on ocean carbon dynamics but are driven more by model assumptions about ocean processes, rather than by direct observational information. They are useful for testing our understanding of oceanographic processes, and importantly have the potential to be used for future projection. Our statistical method provides a complementary observation-based approach to diagnosing carbon trends retrospectively, but has obvious limitations as it can not be used for projection.

In summary, the northwest Atlantic is an important carbon sink, but even in this relatively well-sampled region, available DIC observations in the ocean interior are sparse and have a strong summer sampling bias. To address these challenges, we developed a statistical time series method that generalizes the eMLR approach to allow assessment of non-linear trends and shorter term variability in DIC. Near-surface waters are usually discounted in eMLR analyses due to the high DIC variability associated with the seasonal cycle, however we improved the reliability of anthropogenic carbon estimates in the surface waters (0–200 m) by removing the seasonal cycle that overshadows the variability of anthropogenic carbon. The waters below 1,000 m have usually been analysed on decadal time scales, but our monthly results showed that excess carbon component had a sudden change point in the year 2000, changing from being stationary to increasing at the same rate as the shallower layers. Since 2000, all depths layers were estimated to have the same rate of anthropogenic increase of $\sim 0.57 \mu\text{mol kg}^{-1} \text{ year}^{-1}$.

Current data collection relies on largely opportunistic sampling, which has an inherent and unavoidable amount of spatial and temporal bias. Improvement of ocean sampling schemes should be an important community goal. This work provides a step forward in the challenge of how to use limited and sparse ocean carbon observations so we can produce improved estimation and understanding of ocean carbon and its temporal variations. Future work lies in extending this analysis to include other informative ocean variables related to DIC (e.g., oxygen), better incorporate spatial and depth variations, improve uncertainty quantification and assess and improve spatial and temporal sampling schemes.

Data Availability Statement

Two data sources were used in this work and both are available online. GLODAPv2.2019 data product for the Atlantic Ocean (Key et al., 2015; Olsen et al., 2016, 2019) with data reference (GLODAPv2.2019, 2019) and data available at <https://doi.org/10.25921/xnme-wr20>. GLORYS12v1 reanalysis product with data reference (GLORYS12V1 - Global Ocean Physical Reanalysis Product, 2018) and data available at <https://doi.org/10.48670/moi-00021>. The analysis was performed using R code (R Core Team, 2021) with RStudio (RStudio Teams, 2022), with the assistance of packages for date/time organization: *lubridate* (Grolemund & Wickham, 2011), to load netcdf files: *ncdf4* (Pierce, 2021), for linear model analysis of time-correlated data: *nlme* (Pinheiro et al., 2022), and for assistance with plots: *cmocean* (Thyng et al., 2016), *scales* (Wickham & Seidel, 2021), and *maps* (Becker et al., 2021).

Acknowledgments

We would like to acknowledge Lorenza Raimondi and Dariia Atamanchuk for their many helpful discussions about the eMLR method and anthropogenic carbon. Funding for this research was provided by the Ocean Frontier Institute, National Science and Engineering Research Council of Canada (NSERC) Discovery Grant and the Nova Scotia Graduate Scholarship.

References

- Anderson, B. D. O., & Moore, J. B. (1979). *Optimal filtering*. Prentice-Hall.
- Bakker, D. C. E., Pfeil, B., Landa, C. S., Metzl, N., O'Brien, K. M., Olsen, A., et al. (2016). A multi-decade record of high-quality fCO₂ data in version 3 of the Surface Ocean CO₂ Atlas (SOCAT). *Earth System Science Data*, 8(2), 383–413. <https://doi.org/10.5194/essd-8-383-2016>
- Becker, R. A., Wilks, A. R., Brownrigg, R., Minka, T. P., & Deckmyn, A. (2021). maps: Draw geographical maps. [Software]. Retrieved from <https://CRAN.R-project.org/package=maps>
- Berger, W. H., & Shor, E. N. (2009). *Ocean: Reflections on a century of exploration*. University of California Press.
- Bittig, H. C., Steinhoff, T., Claustre, H., Fiedler, B., Williams, N. L., Sauzède, R., et al. (2018). An alternative to static climatologies: Robust estimation of open ocean CO₂ variables and nutrient concentrations from T, S, and O₂ data using Bayesian Neural Networks. *Frontiers in Marine Science*, 5. <https://doi.org/10.3389/fmars.2018.00328>
- Bostock, H. C., Mikaloff Fletcher, S. E., & Williams, M. J. M. (2013). Estimating carbonate parameters from hydrographic data for the intermediate and deep waters of the Southern Hemisphere oceans. *Biogeosciences*, 10(10), 6199–6213. <https://doi.org/10.5194/bg-10-6199-2013>
- Brewer, P. G., Glover, D. M., Goyet, C., & Shafer, D. K. (1995). The pH of the North Atlantic Ocean: Improvements to the global model for sound absorption in seawater. *Journal of Geophysical Research*, 100(C5), 8761–8776. <https://doi.org/10.1029/95JC00306>
- Broullón, D., Pérez, F. F., Velo, A., Hoppema, M., Olsen, A., Takahashi, T., et al. (2020). A global monthly climatology of oceanic total dissolved inorganic carbon: A neural network approach. *Earth System Science Data*, 12(3), 1725–1743. <https://doi.org/10.5194/essd-12-1725-2020>
- Carroll, D., Menemenlis, D., Dutkiewicz, S., Lauderdale, J. M., Adkins, J. F., Bowman, K. W., et al. (2022). Attribution of space-time variability in global-ocean dissolved inorganic carbon. *Global Biogeochemical Cycles*, 36(3). <https://doi.org/10.1029/2021GB007162>
- Carter, B. R., Feely, R. A., Mecking, S., Cross, J. N., Macdonald, A. M., Siedlecki, S. A., et al. (2017). Two decades of Pacific anthropogenic carbon storage and ocean acidification along Global Ocean Ship-based Hydrographic Investigations Program sections P16 and P02. *Global Biogeochemical Cycles*, 31(2), 306–327. <https://doi.org/10.1002/2016GB005485>
- Ciais, P., Chris, S., Govindasamy, B., Bopp, L., Brovkin, V., Canadell, J., et al. (2013). Carbon and other biogeochemical cycles. In T. F. Stocker, D. Qin, G.-K. Plattner, M. Tignor, S. K. Allen, J. Boschung, et al. (Eds.), *Climate change 2013: The physical science basis. Contribution of Working Group I to the Fifth Assessment Report of the Intergovernmental Panel on Climate Change* (pp. 465–570). Cambridge University Press.
- Clement, D., & Gruber, N. (2018). The eMLR(C*) method to determine decadal changes in the global ocean storage of anthropogenic CO₂. *Global Biogeochemical Cycles*, 32(4), 654–679. <https://doi.org/10.1002/2017GB005819>
- Cressie, N. A. C., & Wikle, C. K. (2011). *Statistics for Spatio-temporal data*. Wiley.
- Drijfhout, S., Oldenborgh, G. J. V., & Cimatoribus, A. (2012). Is a decline of AMOC causing the warming hole above the North Atlantic in observed and modeled warming patterns? *Journal of Climate*, 25(24), 8373–8379. American Meteorological Society Section. <https://doi.org/10.1175/JCLI-D-12-00490.1>
- Emerson, S., & Hedges, J. (2008). *Chemical oceanography and the marine carbon cycle*. Cambridge University Press.
- Emery, W. (2001). Water types and water masses. In *Encyclopedia of ocean sciences* (pp. 3179–3187). Elsevier. <https://doi.org/10.1006/rwos.2001.0108>
- Fassbender, A. J., Rodgers, K. B., Palevsky, H. I., & Sabine, C. L. (2018). Seasonal asymmetry in the evolution of surface ocean pCO₂ and pH thermodynamic drivers and the influence on sea-air CO₂ flux. *Global Biogeochemical Cycles*, 32(10), 1476–1497. <https://doi.org/10.1029/2017GB005855>
- Friedlingstein, P., O'Sullivan, M., Jones, M. W., Andrew, R. M., Hauck, J., Olsen, A., et al. (2020). Global carbon budget 2020. *Earth System Science Data*, 12(4), 3269–3340. <https://doi.org/10.5194/essd-12-3269-2020>
- Friis, K., Körtzinger, A., Pätsch, J., & Wallace, D. W. R. (2005). On the temporal increase of anthropogenic CO₂ in the subpolar North Atlantic. *Deep Sea Research Part I: Oceanographic Research Papers*, 52(5), 681–698. <https://doi.org/10.1016/j.dsr.2004.11.017>
- Fröb, F., Olsen, A., Pérez, F. F., García-Ibáñez, M. I., Jeansson, E., Omar, A., & Lauvset, S. K. (2018). Inorganic carbon and water masses in the Irminger Sea since 1991. *Biogeosciences*, 15(1), 51–72. <https://doi.org/10.5194/bg-15-51-2018>
- Gerber, M., & Joos, F. (2010). Carbon sources and sinks from an Ensemble Kalman Filter ocean data assimilation. *Global Biogeochemical Cycles*, 24(3). <https://doi.org/10.1029/2009GB003531>
- GLODAPv2.2019. (2019). [Dataset]. <https://doi.org/10.25921/xnme-wr20>
- GLORYS12V1 - Global Ocean Physical Reanalysis Product. (2018). [Dataset]. <https://doi.org/10.48670/moi-00021>
- Goddijn-Murphy, L. M., Woolf, D. K., Land, P. E., Shutler, J. D., & Donlon, C. (2015). The OceanFlux Greenhouse Gases methodology for deriving a sea surface climatology of CO₂ fugacity in support of air–sea gas flux studies. *Ocean Science*, 11(4), 519–541. <https://doi.org/10.5194/os-11-519-2015>
- Grolemund, G., & Wickham, H. (2011). Dates and times made easy with lubridate. *Journal of Statistical Software*, 40(3), 1–25. <https://doi.org/10.18637/jss.v040.i03>
- Gruber, N., Clement, D., Carter, B. R., Feely, R. A., van Heuven, S., Hoppema, M., et al. (2019). The oceanic sink for anthropogenic CO₂ from 1994 to 2007. *Science*, 363(6432), 1193–1199. <https://doi.org/10.1126/science.aau5153>
- Gruber, N., Keeling, C. D., & Bates, N. R. (2002). Interannual variability in the North Atlantic Ocean carbon sink. *Science*, 298(5602), 2374–2378. <https://doi.org/10.1126/science.1077077>
- Holfort, J., Johnson, K. M., Schneider, B., Siedler, G., & Wallace, D. W. R. (1998). Meridional transport of dissolved inorganic carbon in the South Atlantic Ocean. *Global Biogeochemical Cycles*, 12(3), 479–499. <https://doi.org/10.1029/98GB01533>
- Keppeler, L., Landschützer, P., Gruber, N., Lauvset, S. K., & Stemmler, I. (2020). Seasonal carbon dynamics in the near-global ocean. *Global Biogeochemical Cycles*, 34(12). <https://doi.org/10.1029/2020GB006571>
- Key, R. M., Olsen, A., van Heuven, S., Lauvset, S. K., Velo, A., Schirnick, C., et al. (2015). Global Ocean Data Analysis Project, Version 2 (GLODAPv2).
- Khatiwal, S., Tanhua, T., Mikaloff Fletcher, S., Gerber, M., Doney, S. C., Graven, H. D., et al. (2013). Global ocean storage of anthropogenic carbon. *Biogeosciences*, 10(4), 2169–2191. <https://doi.org/10.5194/bg-10-2169-2013>
- Koelling, J., Atamanchuk, D., Karstensen, J., Handmann, P., & Wallace, D. W. R. (2022). Oxygen export to the deep ocean following Labrador Sea Water formation. *Biogeosciences*, 19(2), 437–454. <https://doi.org/10.5194/bg-19-437-2022>
- Lacour, L., Briggs, N., Claustre, H., Ardyna, M., & Dall'Olmo, G. (2019). The intraseasonal dynamics of the mixed layer pump in the subpolar North Atlantic Ocean: A biogeochemical-argo float approach. *Global Biogeochemical Cycles*, 33(3), 266–281. <https://doi.org/10.1029/2018GB005997>
- Laine, M. (2020). Introduction to dynamic linear models for time series analysis. In J.-P. Montillet & M. S. Bos (Eds.), *Geodetic time series analysis in earth sciences. Springer Geophysics* (pp. 139–156). Springer International Publishing. https://doi.org/10.1007/978-3-030-21718-1_4

- Landschützer, P., Gruber, N., Bakker, D. C. E., & Schuster, U. (2014). Recent variability of the global ocean carbon sink. *Global Biogeochemical Cycles*, 28(9), 927–949. <https://doi.org/10.1002/2014GB004853>
- Landschützer, P., Gruber, N., Bakker, D. C. E., Schuster, U., Nakaoka, S., Payne, M. R., et al. (2013). A neural network-based estimate of the seasonal to inter-annual variability of the Atlantic Ocean carbon sink. *Biogeosciences*, 10(11), 7793–7815. <https://doi.org/10.5194/bg-10-7793-2013>
- Lauvset, S. K., Key, R. M., Olsen, A., van Heuven, S., Velo, A., Lin, X., et al. (2016). A new global interior ocean mapped climatology: the 1°×1° GLODAP version 2. *Earth System Science Data*, 8(2), 325–340. <https://doi.org/10.5194/essd-8-325-2016>
- Lauvset, S. K., Lange, N., Tanhua, T., Bittig, H. C., Olsen, A., Kozyr, A., et al. (2021). An updated version of the global interior ocean biogeochemical data product, GLODAPv2.2021. *Earth System Science Data*, 13, 5565–5589. Copernicus GmbH. <https://doi.org/10.5194/essd-13-5565-2021>
- Levine, N. M., Doney, S. C., Lima, I., Wanninkhof, R., Bates, N. R., & Feely, R. A. (2011). The impact of the North Atlantic Oscillation on the uptake and accumulation of anthropogenic CO₂ by North Atlantic Ocean mode waters. *Global Biogeochemical Cycles*, 25(3). <https://doi.org/10.1029/2010GB003892>
- Longhurst, A. (2007). *Ecological geography of the sea*. Elsevier. <https://doi.org/10.1016/B978-0-12-455521-1.X5000-1>
- Macdonald, A., Baringer, M., Wanninkhof, R., Lee, K., & Wallace, D. (2003). A 1998–1992 comparison of inorganic carbon and its transport across 24.5°N in the Atlantic. *Deep Sea Research Part II: Topical Studies in Oceanography*, 50(22–26), 3041–3064. <https://doi.org/10.1016/j.dsr2.2003.07.009>
- Mackay, N., Watson, A. J., Suntharalingam, P., Chen, Z., & Landschützer, P. (2022). Improved winter data coverage of the Southern Ocean CO₂ sink from extrapolation of summertime observations. *Communications Earth & Environment*, 3(1), 265. <https://doi.org/10.1038/s43247-022-00592-6>
- McKinley, G. A., Fay, A. R., Lovenduski, N. S., & Pilcher, D. J. (2017). Natural variability and anthropogenic trends in the ocean carbon sink. *Annual Review of Marine Science*, 9(1), 125–150. <https://doi.org/10.1146/annurev-marine-010816-060529>
- Montes-Hugo, M., Sweeney, C., Doney, S. C., Ducklow, H., Frouin, R., Martinson, D. G., et al. (2010). Seasonal forcing of summer dissolved inorganic carbon and chlorophyll a on the Western shelf of the Antarctic Peninsula. *Journal of Geophysical Research*, 115(C3), C03024. <https://doi.org/10.1029/2009JC005267>
- North Atlantic Oscillation. (2005). [Dataset]. Retrieved from <https://www.cpc.ncep.noaa.gov/products/precip/CWlink/pna/nao.shtml>
- Olsen, A., Key, R. M., van Heuven, S., Lauvset, S. K., Velo, A., Lin, X., et al. (2016). The Global Ocean Data Analysis Project version 2 (GLODAPv2) – An internally consistent data product for the world ocean. *Earth System Science Data*, 8(2), 297–323. <https://doi.org/10.5194/essd-8-297-2016>
- Olsen, A., Lange, N., Key, R. M., Tanhua, T., Álvarez, M., Becker, S., et al. (2019). GLODAPv2.2019 – An update of GLODAPv2. *Earth System Science Data*, 11(3), 1437–1461. <https://doi.org/10.5194/essd-11-1437-2019>
- Pierce, D. (2021). ncd4: Interface to Unidata netCDF (version 4 or earlier) format data files. [Software]. Retrieved from <https://CRAN.R-project.org/package=ncdf4>
- Pinheiro, J., Bates, D., DebRoy, S., Sarkar, D., EISPACKEHeisterkamp, S., & R Core Team. (2022). nlme: Linear and Nonlinear Mixed Effects Models. [Software]. Retrieved from <https://CRAN.R-project.org/package=nlme>
- Plancherel, Y., Rodgers, K. B., Key, R. M., Jacobson, A. R., & Sarmiento, J. L. (2013). Role of regression model selection and station distribution on the estimation of oceanic anthropogenic carbon change by eMLR. *Biogeosciences*, 10(7), 4801–4831. <https://doi.org/10.5194/bg-10-4801-2013>
- Raimondi, L., Tanhua, T., Azetsu-Scott, K., Yashayaev, I., & Wallace, D. (2021). A 30-year time series of transient tracer-based estimates of anthropogenic carbon in the Central Labrador Sea. *Journal of Geophysical Research: Oceans*, 126(5), e2020JC017092. <https://doi.org/10.1029/2020JC017092>
- R Core Team. (2021). R: A language and environment for statistical computing. [Software]. Retrieved from <https://www.R-project.org/>
- Rödenbeck, C., Bakker, D. C. E., Gruber, N., Iida, Y., Jacobson, A. R., Jones, S., et al. (2015). Data-based estimates of the ocean carbon sink variability – First results of the Surface Ocean pCO₂ mapping intercomparison (SOCOM). *Biogeosciences*, 12(23), 7251–7278. <https://doi.org/10.5194/bg-12-7251-2015>
- Rödenbeck, C., Keeling, R. F., Bakker, D. C. E., Metzl, N., Olsen, A., Sabine, C., & Heimann, M. (2013). Global surface-ocean pCO₂ and sea-air CO₂ flux variability from an observation-driven ocean mixed-layer scheme. *Ocean Science*, 9(2), 193–216. <https://doi.org/10.5194/os-9-193-2013>
- RStudio Teams. (2022). RStudio: Integrated Development Environment for R. [Software]. Retrieved from <http://www.rstudio.com/>
- Rühs, S., Oliver, E. C. J., Biastoch, A., Böning, C. W., Dowd, M., Getzlaff, K., et al. (2021). Changing spatial patterns of deep convection in the subpolar North Atlantic. *Journal of Geophysical Research: Oceans*, 126(7). <https://doi.org/10.1029/2021JC017245>
- Sabine, C. L., Feely, R. A., Gruber, N., Key, R. M., Lee, K., Bullister, J. L., et al. (2004). The oceanic sink for anthropogenic CO₂. *Science*, 305(5682), 367–371. <https://doi.org/10.1126/science.1097403>
- Sabine, C. L., & Tanhua, T. (2010). Estimation of anthropogenic CO₂ inventories in the ocean. *Annual Review of Marine Science*, 2(1), 175–198. <https://doi.org/10.1146/annurev-marine-120308-080947>
- Sathyanarayanan, A., Köhl, A., & Stammer, D. (2021). Ocean Salinity changes in the global ocean under global warming conditions Part 1: Mechanisms in a strong warming scenario. *Journal of Climate*, 1–56. <https://doi.org/10.1175/JCLI-D-20-0865.1>
- Tanhua, T., & Keeling, R. F. (2012). Changes in column inventories of carbon and oxygen in the Atlantic Ocean. *Biogeosciences*, 9(11), 4819–4833. <https://doi.org/10.5194/bg-9-4819-2012>
- Thacker, W. C. (2012). Regression-based estimates of the rate of accumulation of anthropogenic CO₂ in the ocean: A fresh look. *Marine Chemistry*, 132–133, 44–55. <https://doi.org/10.1016/j.marchem.2012.02.004>
- Thomas, H., Friederike Prowe, A. E., Lima, I. D., Doney, S. C., Wanninkhof, R., Greatbatch, R. J., et al. (2008). Changes in the North Atlantic Oscillation influence CO₂ uptake in the North Atlantic over the past 2 decades. *Global Biogeochemical Cycles*, 22(4). <https://doi.org/10.1029/2007GB003167>
- Thyng, K., Greene, C., Hetland, R., Zimmerle, H., & DiMarco, S. (2016). True colors of oceanography: Guidelines for effective and accurate colormap selection. *Oceanography*, 29(3), 9–13. <https://doi.org/10.5670/oceanog.2016.66>
- Turk, D., Dowd, M., Lauvset, S. K., Koelling, J., Alonso-Pérez, F., & Pérez, F. F. (2017). Can empirical algorithms successfully estimate aragonite saturation state in the subpolar North Atlantic? *Frontiers in Marine Science*, 4. <https://doi.org/10.3389/fmars.2017.00385>
- Ullman, D. J., McKinley, G. A., Bennington, V., & Dutkiewicz, S. (2009). Trends in the North Atlantic carbon sink: 1992–2006. *Global Biogeochemical Cycles*, 23(4). <https://doi.org/10.1029/2008GB003383>
- Wallace, D. W. R. (1995). *Monitoring global ocean carbon inventories*. Ocean Observing System Development Panel, Texas A&M University.

- Wallace, D. W. R. (2001). Introduction to special section: Ocean measurements and models of carbon sources and sinks. *Global Biogeochemical Cycles*, *15*(1), 3–10. <https://doi.org/10.1029/2000GB001354>
- Wickham, H., & Seidel, D. (2021). scales: Scale Functions for Visualization. [Software]. Retrieved from <https://CRAN.R-project.org/package=scales>
- Zivot, E., & Wang, J. (2003). State space models. In *Modeling financial time series with S-Plus®* (pp. 499–542). Springer New York. https://doi.org/10.1007/978-0-387-21763-5_14